Z. Phys. C 66, 417–428 (1995)

ZEITSCHRIFT
FÜR PHYSIK C

Determination of the atmospheric neutrino spectra with the Fréjus detector

Fréjus Collaboration

K. Daum[4,*], W. Rhode[4], P. Bareyre[3], R. Barloutaud[3], G. Chardin[3], B. Degrange[2], J. Ernwein[3], B. Kuznik[4], H. Meyer[4], L. Mosca[3], L. Moscoso[3], O. Perdereau[1], M. Schubnell[4,**], S. Tisserant[2,***], Y. Wei[4]

[1] Paris-Sud, IN2P3-CNRS, Orsay, France
[2] LPNHE, Ecole Polytechnique, IN2P3-CNRS, Palaiseau, France
[3] CEA, DSM, DAPNIA/SPP, C.E. Saclay, 91191 Gif-sur-Yvette, France
[4] Fachbereich Physik, Bergische Universität Gesamthochschule Wuppertal, Wuppertal, Germany[a]

Received: 2 February 1995

Abstract. The combined analysis of the final event set of data on neutrino interactions inside the detector, upward going stopping muons and horizontal muons recorded in the Fréjus experiment is presented. The absolute atmospheric neutrino spectra in the energy range 320 MeV $< E_{\nu_e} <$ 30 GeV for electron neutrinos and 250 MeV$< E_{\nu_\mu} <$ 10 TeV for muon neutrinos are determined. Based on the parameterization of Volkova for the ν_μ-flux a spectral index of $\gamma = 2.66 \pm 0.05$ is obtained from the ratio of horizontal muons over upward going stopping muons and from the measurement of the energy loss of horizontal muons inside the detector. The neutrino spectra are compared with various flux calculations. They do not show any evidence for neutrino oscillations in agreement with earlier analyses of the Fréjus data.

1 Introduction

During the past decade the interest in a better knowledge of the atmospheric neutrino spectra increased considerably in various fields of particle physics as well as in astrophysics. A good understanding of atmospheric neutrino flux and the detailed dynamics of neutrino interactions was primarily needed by the deep underground nucleon decay experiments [1-7] in order to improve the confidence in background studies in nucleon decay searches. Results on atmospheric neutrinos are published by most of the experiments [8-13].

A good knowledge of the atmospheric neutrino flux has also become mandatory due to the increasing experimental activities in the field of high energy neutrino astronomy [14]. The ultimate sensitivity of these experiments to astrophysical neutrino sources will be limited by the atmospheric neutrino background. Up to now only theoretical calculations [15-21] of the absolute atmospheric neutrino spectra exist.

The study of atmospheric neutrinos also allows to search for neutrino oscillations in a region of the parameter space not accessible by any other means so far. Using the contained single ring events the Kamiokande experiment reported on a deficit of muon type neutrino interactions in their detector [9]. This observation was later confirmed with larger statistics [12] as well as by the IMB experiment [13] and was attributed to neutrino oscillations by the Kamiokande collaboration. Furthermore Kamiokande reported recently on evidence for an abnormal ratio of muon type over electron type neutrino interactions in their apparatus at higher neutrino energies [22] [1]. In contrast the iron calorimeter experiments NUSEX and Fréjus [10, 11, 23] observe the predicted rate of ν_μ-interactions using the full neutrino data sample while Soudan-II gave preliminary evidence for a ν_μ-deficit based on the quasi-elastic ν-interactions only [24]. The analyses of upward-going, horizontal or stopping muons [25, 26, 27] predominantly stemming from deep inelastic ν_μ-interactions in the rock again do not show any indication for neutrino oscillations in the region of the parameter space consistent with the Kamiokande observation on contained and semi-contained events.

In this paper the analysis of neutrino interactions inside the detector in combination with the upward-going stopping and horizontal muons produced by ν_μ-interactions in the surrounding rock recorded in the Fréjus experiment is presented. The spectra are inferred from the data with help of the regularized unfolding method [28] for both the observed neutrino interactions inside the detector and the ν_μ-induced muons. The fine granularity of the Fréjus detector allows to measure the stochastic energy loss of muons well below their energy loss due to ionization for a mean muon track . It is this unique feature of the detector which enables us to measure the absolute ν_μ spectrum up to 10 TeV for the first time. The absolute neutrino spectra are compared with different theoretical flux calculations.

* Present address: DESY, Hamburg, Germany,
e-mail: daum@vxdesy.desy.de
** Now at: University of Michigan, Ann Arbor, USA
*** Now at: CPPM, Faculté des Sciences de Luminy, F-13288, Marseille Cedex 9, France
[a] Supported by the Bundesministerium für Forschung und Technologie, FRG under contract number 55WT84P

[1] Due to the detection technique the water Cerenkov experiments have to restrict their analyses mainly to single ring events which are dominated by quasielastic νN-scattering events.

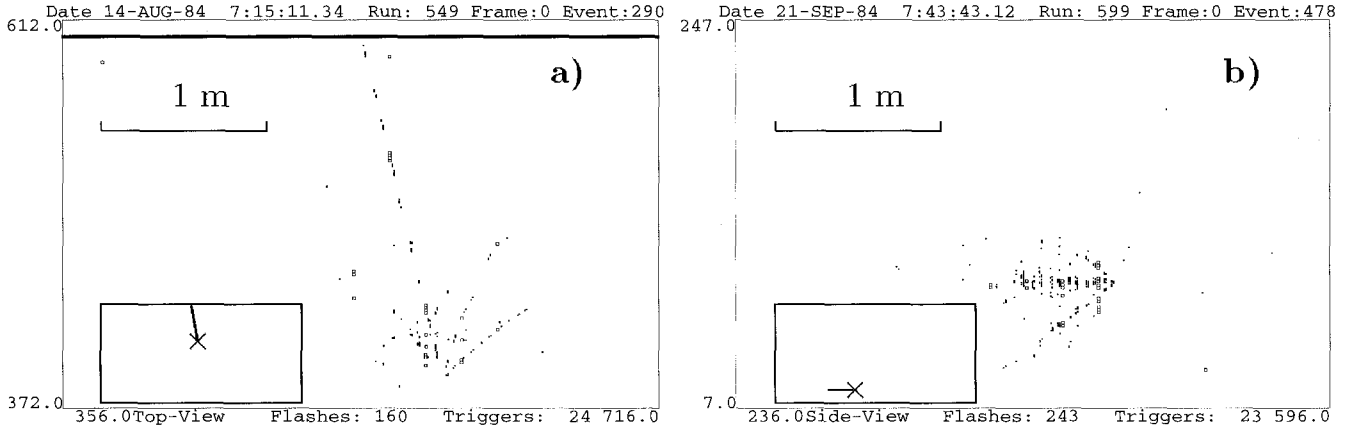

Fig. 1. Two deep inelastic scattering neutrino events as observed in the Fréjus detector: (a) semicontained ν_μ-interaction with $E_{vis} \approx 3.1$ GeV, (b) contained ν_e-interaction with $E_{vis} \approx 3.9$ GeV. The vertex positions and the direction of the summed momenta are indicated in the insert.

2 Site and experiment

The Fréjus underground laboratory is located near the center of the highway tunnel connecting Modane (France) to Bardonecchia (Italy) under the Alps. The average rock overburden amounts to 1720 m corresponding to 4710 hg/cm^2 [29]. The geological structure is quite homogeneous in a large area [30]. Characteristics of the Fréjus rock and details of the topological structure also crucial for this analysis are given in ref. [31]. The geographical coordinates of the site are $45^o 8' 32''$ north and $6^o 41' 21''$ east corresponding to a geomagnetic latitude of 44.5^o.

The detector has been described in detail in ref. [32]. It is a high resolution iron calorimeter with a total mass of 900 tons measuring 6m×6m×12.3m. The fine granularity is achieved by a sandwich structure consisting of 912 flash chambers (5mm×5mm cells) and iron (3mm) planes interspersed with 113 planes of Geiger tubes (15mm×15mm cells) which provide the trigger. The detector cells are oriented vertical and horizontal alternately, thus providing two independent orthogonal views for each event.

The response of the Fréjus detector to electrons and pions has been calibrated with a test detector exposed to particle beams at the electron synchrotrons of DESY and Bonn university [32]. The behavior of low energetic muons has been studied by the atmospheric stopping muons. From the analysis of the test detector data and of the decay of positively charged stopping muons an energy threshold of about 30 MeV has been inferred for the detection of electromagnetic showers induced by photons or electrons. The energy resolution is described by

$$\frac{\sigma(E)}{E} = 0.055 + \frac{0.06}{\sqrt{E\,[\mathrm{GeV}]}} \qquad (1)$$

with an accuracy of about 10%. This relation also holds for the electromagnetic energy loss of through going muons, for which an effective detection threshold for pair production and bremsstrahlung of 0.15 MeV g^{-1} cm^2 is obtained.

The trigger requires groups of hits in the Geiger counters in a small volume (1m^3) corresponding to a threshold of 200 MeV in electromagnetic energy or, equivalently, to a track length of about 100 g/cm^2. The efficiency of the detector was constantly monitored by analyzing the atmospheric muons passing through the apparatus. The average trigger rate is about 45 events per hour. Half of the triggers are due to atmospheric muons while the rest is induced by local radioactivity and electronic noise. The event rate produced by interactions of atmospheric neutrinos is on the order of one event per week.

3 Data processing

Continuous data taking started February 19, 1984 with a mass of 240 tons. The size of the detector was gradually increased until the final mass of 900 tons was reached in June 1985. Data taking ended September 13, 1988. This analysis is based on neutrino interactions inside the fiducial volume of the detector, which are classified as contained or semicontained events, upward going stopping muons and horizontal through-going muons.

3.1 Neutrino interactions inside the detector

An event is defined to be contained if no prong (track or shower) is leaving the detector taking into account the detector geometry and the cell efficiency. An event is classified to be semicontained if a possible primary vertex is found inside the detector and at least one prong is leaving the apparatus. The selection of contained and semicontained events starts during data taking when the physicist on shift scans all events and classifies them according to simple selection rules. Subsequently an independent off line selection is performed with help of a pattern recognition program. The combined efficiency to select neutrino induced events is found to be 98%.

In order to reduce the possible background due to photons and neutral hadrons entering the detector a fiducial cut is applied to the events. Thus a minimum distance of 25 cm for any vertex with respect to the surface of the detector is required. This reduces the fiducial mass to 700 tons leading

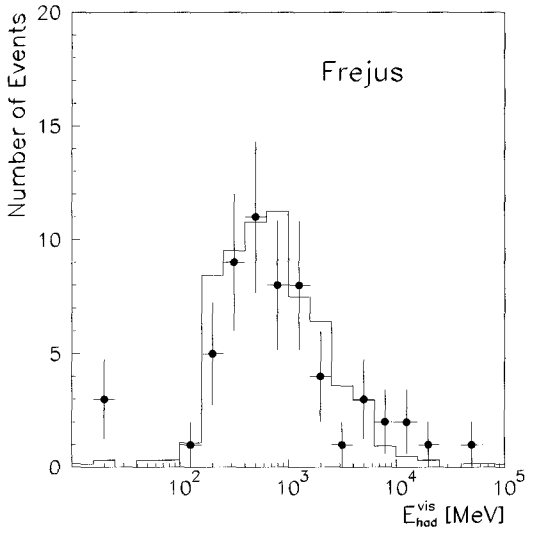

Fig. 2. Distribution of the visible hadronic energy E_{had}^{vis} of semicontained events in comparison to the absolute Monte Carlo expectation of neutrino interactions in the detector.

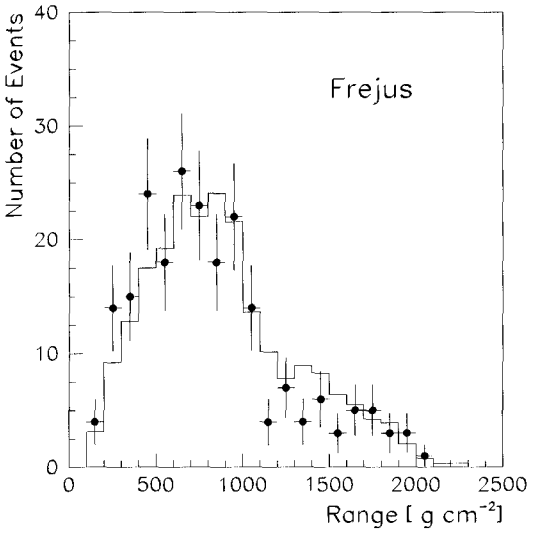

Fig. 3. Potential path distribution of the range between the interaction point and the entrance point of the neutrino into the detector. The neutrino direction is assumed to coincide with the direction of the total visible momentum. In the Fréjus detector one radiation length and one nuclear interaction length correspond to $\approx$ 14 g cm^{-2} and $\approx$ 135 g cm^{-2}, respectively.

to an exposure of 2.0 kiloton year (kty). With this cut we select 158 fully contained events and 58 semicontained events with at least two prongs [2].

A pattern recognition program [23, analysis 2] is applied for event reconstruction. Only the vertices of the events are determined visually on a graphic terminal while track finding, association of tracks in the two independent views, particle identification (shower or track) and momentum determination and classification as charged current ν_μ or ν_e and neutral current interaction is done by the analysis program. Details on this classification are given in ref. [11]. As an example for ν_e and ν_μ interactions two deep inelastic scattering events are shown in Fig. 1. For about 5% of the events the correlation of tracks in the two independent views is not unique leading to different event definitions which may also lead to different neutrino interpretations albeit to a much smaller extent (less than one event). In case of ambiguities all hypotheses are used in the analysis.

Because of the detection technique applied in the Fréjus experiment it is not necessary to restrict our analysis of neutrino interactions inside the apparatus to fully contained events only, although the potential Background due to charged particles entering the detector and producing a vertex by interaction or decay may present has to be considered. As a check of the purity of the selection of semicontained neutrino interactions the distribution of the visible hadronic energy

$$E_{had}^{vis} = E_{vis} - E_{lepton}^{vis} \tag{2}$$

is shown in Fig. 2 for the data in comparison with expectation from simulated neutrino interactions. Here E_{vis} denotes the visible energy of the events while E_{lepton}^{vis} is the measured energy of the particles defined as lepton according to the procedure described in ref. [11]. The data is in good agreement with the absolute Monte Carlo prediction. In particular we do not observe any significant excess of events at energies $E_{had}^{vis} < 100$ MeV which would be present in case of contaminations due to atmospheric stopping muons with decay electrons in this event sample[3].

Furthermore the selection of neutrino interactions inside the detector may be contaminated by entering photons or neutral hadrons being produced by atmospheric muons interacting in the rock surrounding the detector. To estimate the contribution of these particles to our event selection the neutrino path length between the interaction point and the reconstructed entrance point of the neutrino into the detector is shown in Fig. 3 for the contained and semicontained events. It is assumed that the neutrino direction is given by the vector of the total visible momentum. A contamination of the data by entering neutral particles different from neutrinos should become visible as an excess of events at very small values for the potential path length. Again good agreement between our data and the absolute prediction of the atmospheric neutrino Monte Carlo is observed. Especially we do not observe any event below 150 g cm^{-2} which corresponds to more than one nuclear interaction length and more than 10 radiation lengths in our detector. For comparison the fiducial cut corresponds to a minimum range of 50 g cm^2. Taking into account the fiducial cut the absence of events with vertex closer than 150 g cm^{-2} to the surface of the detector leads to an upper limit on a contamination of the neutrino sample due to neutral hadrons of less than four events at 95% C.L. We therefore feel confident that both the semicontained events and fully contained events are only induced by neutrinos interacting inside the apparatus.

[2] Since the Fréjus detector has except by energy loss no capabilities to determine the direction of tracks the down(up)ward-going stopping muons cannot be distinguished from the single muon up(down)ward-going events, we have excluded from this data sample the ν-interactions producing single prong events leaving the detector.

[3] In the data we observe three events with $E_{had}^{vis} < 100$ MeV compared to a Monte Carlo expectation of one event. In two of these events a track is leaving the detector while the remaining one has an uncontained shower.

3.2 Neutrino induced muons

The selection and reconstruction of the upward-going stopping muons and the through-going muons is done by the same pattern recognition program as used for the offline selection of contained and semicontained events. Following the track finding routine the program searches for showers along the muon track due to pair production, bremsstrahlung and hadron production and determines the shower energies, the shower multiplicity and the total energy loss due to these processes including the contribution of unresolved low energetic showers.

Stopping muons are defined by the following criteria: (a) the maximum distance of the reconstructed entrance point of the muon from the detector surface has to be less than 30 cm and (b) the distance of the reconstructed stopping point of the track from the detector surface has to be at least 30 cm. The decision whether a track is directed upward or downward is found by the determination of the direction entrance point.

In order to obtain a sufficient pointing accuracy to the origin of the muons a minimum track length of 1 m in three dimensional space is required. Further details on the processing of this data sample are given in ref. [33].

Subsequently the depth with intensity relationship is investigated in order to separate the neutrino induced muons from the overwhelming background of atmospheric muons. For a given direction the muon intensity is corrected for acceptance, runtime of the experiment and dependence on the zenith angle. According to the direction of the muons the rock overburden is calculated from the mountain profile given in ref. [31, 34]. The depth intensity curve is given in [31, 33]. By allowing for an expected contamination of one event from atmospheric muons in the neutrino induced horizontal muon sample a cut equivalent to a depth of 14000 hg/cm^2 is applied. Taking into account the ambiguity in the direction of the muons the corresponding solid angle is 2.3 sr for through-going muons and 7.43 sr for semicontained one track events subsequently quoted as upward-going stopping muons. With this cut 44 quasi horizontal and 48 upward-going stopping muons which are assumed to be neutrino induced are selected. In the latter event sample a contamination of 11 events due to misidentified atmospheric downward-going muons is expected from Monte Carlo simulations of atmospheric muons.

4 Simulation of neutrino interactions

According to the classification of the events into neutrino interactions inside and outside the detector two different Monte Carlo programs are needed in this analysis. In both cases the atmospheric neutrino flux is based on the calculations according to ref. [16] for $E_\nu \leq 3$ GeV and according to ref. [15] for $E_\nu \geq 3$ GeV.

For the analysis of contained and semicontained events the neutrino Monte Carlo described in ref. [11] is used. Nuclear effects are treated in an intranuclear cascade model with off-shell nucleons in a Fermi gas using the local density approach [35, model B]. We have simulated neutrino interactions corresponding to a sensitivity of 12.8 kty. The events are passed through the same analysis chain as described in the previous section. The simulation of the kinematics at the neutrino vertex and the reinteraction of produced hadrons has been checked by a reanalysis [36] of a subsample of the data recorded by the Aachen-Padova neutrino experiment [37].

For the study of muons induced by neutrino interactions in the rock a Monte Carlo program specifically tailored to this purpose is developed. As in the previous case it includes the quasielastic scattering, the single pion production and the deep inelastic scattering of neutrinos as described in ref [11]. For deep inelastic scattering events the kinematics of the muon is given by the nucleon structure function which is parametrized according to EHLQ [38]. Although more recent calculations [39] on the proton structure function as well as new measurements from HERA [40] exist it is sufficient to consider the EHQL parametrization here since the analysis is nearly independent of the behaviour of the nuclear structure function for $x \leq 10^{-2}$. We have studied in detail the influence of different parametrizations [39]. Only small variations due to the different models well below 10% are observed.

Subsequently the total energy loss of the muon in the rock is approximated by

$$-\frac{dE}{dx} = a + b \cdot E \tag{3}$$

where $a = (2.17 \pm 0.04) \cdot 10^{-3}$ GeV g^{-1} cm^2 and $b = (4.12 \pm 0.16) \cdot 10^{-6}$ g^{-1} cm^2 are parameters which define the energy losses due to ionization and the sum of pair production, knock-on electrons, bremsstrahlung and photonuclear reactions, respectively. These parameters are determined by the atmospheric muon data of Fréjus in a combined analysis of the depth intensity relation, the ratio of stopping over through-going atmospheric muons and the measurement of the energy loss of through-going muons inside the detector [29]. Finally the neutrino induced muons reaching the detector are passed through the detector simulation program and through the analysis chains described in the previous section.

In order to be able to determine the atmospheric neutrino spectra various sets of simulated data with different spectral indices for the parametrization of ref [15] are generated. The data of each simulation corresponds to a runtime of 100 years of the full-sized detector.

5 Neutrino flux

The determination of the atmospheric neutrino spectra is based on four different experimental ingredients, namely

a) the rate and energy dependence of the contained and semicontained events,
b) the ratio $r_{hori}^{cont} = (n_{cont} + n_{semi})/n_{hori}$ of the contained and semicontained charged current ν_μ events over the horizontal through-going muons,
c) the ratio $r_{hori}^{stop} = n_{stop}/n_{hori}$ of the upward-going stopping muons over the horizontal through-going muons and
d) the distribution of the visible energy loss of through-going muons.

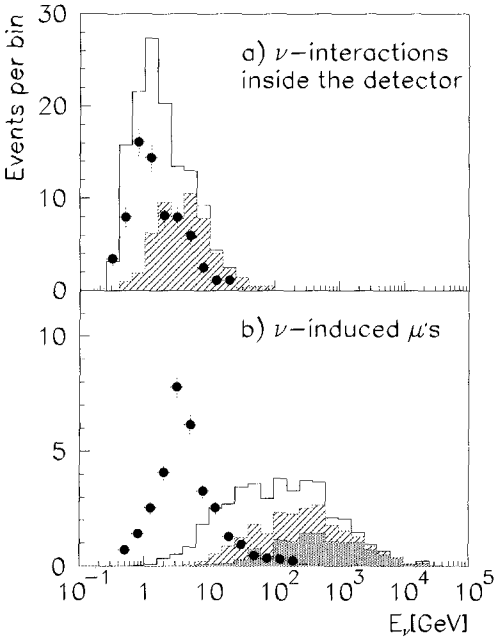

Fig. 4. Monte Carlo expectation for the neutrino energy distributions accessible by the different event classes: a) for ν-interactions inside the detector, the dots (histogram) show the energy distribution for ν_e (ν_μ)-interactions while the hatched histogram indicates the contribution of semicontained ν_μ-events, and b) for the neutrino induced muons where the dots (histogram) correspond to the expectation for upward-going stopping muons (horizontal through-going muons). The hatched (grey) area indicate the contribution to the horizontal through-going muons from muon tracks with a total stochastic energy loss of more than 100(500) MeV inside the detector. The event rates are normalized to the sensitivity of the Fréjus experiment.

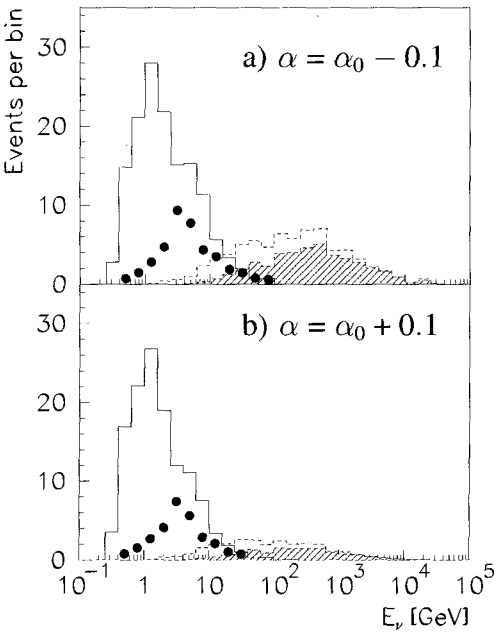

Fig. 5. Monte Carlo expectation for the neutrino energy distributions accessible by the contained and semicontained events (full line), the upward-going stopping muons (black dots) and horizontal muons (dashed line) for different values of the spectral index α. The hatched area indicate the contribution to the horizontal through-going muons from muon tracks with a total stochastic energy loss of more than 100 MeV inside the detector.

Table 1. Comparison of the data and Monte Carlo sample composition. The Monte Carlo predictions are given for three different values of the spectra index α and a fixed value of Φ_0. The values of α_0 and Φ_0 are given in Ref. [14,16].

	Data	MC		
		α_0	$\alpha_0+0.1$	$\alpha_0-0.1$
CC ν_e	75	81.4	75.6	88.2
CC ν_μ	125	136.2	128.5	145.8
NC	16	14.5	13.9	15.4
μ^{up}	48	58.4	53.4	63.9
μ^{hori}	44	43.9	27.6	72.4

To see the advantage of the combined analysis of the different event classes for the determination of the atmospheric neutrino spectra the effect of the slope of the neutrino spectra will be discussed in some detail.

Figure 4 shows the Monte Carlo expected energy distribution derived from the calculations of Ref. [15, 16]and including trigger and acceptance cuts, for the various event categories. The energy distribution of the contained and semicontained events allows a direct measurement of the atmospheric neutrino spectra for 300 MeV$\leq E_\nu \leq$ 50 GeV. For this event class the mean value of the neutrino energy is roughly $\langle E_\nu \rangle \approx$ 1, 2, 4 GeV for the contained ν_μ events, the ν_e interactions and the semicontained ν_μ events, respectively. The differences in $\langle E_\nu \rangle$ for the contained ν_μ and ν_e events is due to the fact that the length of the muon track rises linearly with energy while the length of an electromagnetic shower increases only like $\ln E_e$. Therefore the containment requirements as defined in [11] affect ν_μ and ν_e interactions quite differently.

The upward-going stopping muons cover the energy range 1 GeV$\leq E_{\nu_\mu} \leq$ 50 GeV with a mean value of $\langle E_\nu \rangle \approx 5$ GeV. This energy range is covered independently by the contained and semicontained events. The horizontal through-going muons are due to neutrino interactions in the rock with 5 GeV $\leq E_\nu \leq$ 20 TeV having a mean value of $\langle E_\nu \rangle \approx 100$ GeV. Again, there exists an overlap in E_{ν_μ} with the semicontained events for this data.

Due to the power law spectra of the primary cosmic ray particles the neutrino spectra may be approximated by

$$\Phi_\nu(E_\nu, \lambda, \Theta, \phi) = \Phi_0 \, E_\nu^{-\alpha} \, f_\nu(E_\nu, \lambda, \Theta, h(\Theta, \phi)). \quad (4)$$

The function f_ν describes the deviation of the neutrino spectra from a simple power law. It accounts for the π, K and μ spectra produced in the atmospheric cascade and for the geomagnetic cut off. At low energies this cut off depends on the geomagnetic latitude λ of the experiment.At higher energies the function f_ν takes into account the competition between interaction and decay of π's and K's and the free muon decay length, which depends on the geographical topology $h(\Theta, \phi)$ at the site of the experiment. The topology is a function of the zenith and azimuth angles Θ and ϕ, respectively.

The effect of the variation of the spectral index α on the neutrino energy distribution as observed in the different event classes is show in Fig. 5. For the contained and semicontained events the change in the energy distribution is obvious. While the stopping muon sample measures the

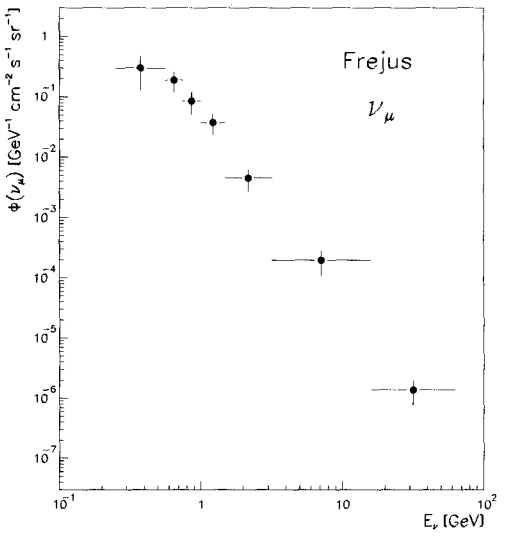

Fig. 6. The absolute ν_μ-spectrum obtained from the contained and semi-contained ν_μ interactions in the Fréjus detector averaged over the zenith angle.

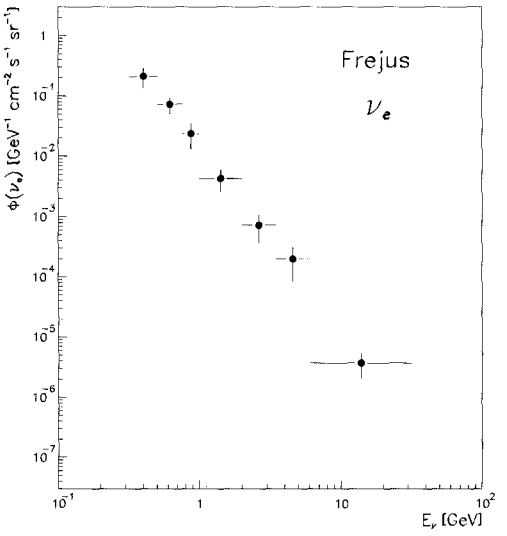

Fig. 7. The absolute ν_e-spectrum obtained from the contained ν_e-interactions in the Fréjus detector averaged over the zenith angle.

spectrum of the neutrino induced muons at the detector for $E_\nu \approx 5$ GeV the through-going muon rate is sensitive to the integrated neutrino flux mainly for $E_\nu > 10$ GeV. As a result the ratio r_{hori}^{stop} shows a positive correlation with the spectral index α of the atmospheric ν_μ spectrum. The mean energy of the horizontal muons observed in the detector decreases when the slope of the atmospheric ν_μ distribution increases. Therefore the probability to observe showers along the muon track in the detector and the mean energy per shower is negatively correlated with the spectral index α of the ν_μ spectrum.

The statistics of the different event classes is compared to the Monte Carlo expectation in Tab. 1. For each event sample we find good agreement between the number of observed events and the Monte Carlo prediction based on the neutrino flux calculations of Ref. [15, 16] taken at a mean solar activity which is appropriate for the data taking time of the Fréjus experiment. If we call n_μ and n_e the number of identified ν_μ and ν_e induced events, respectively, the double ratio

$$R = \frac{(n_\mu/n_e)_{data}}{(n_\mu/n_e)_{MC}} = 1.00 \pm 0.15 \text{ (stat.)} \pm 0.08 \text{ (syst.)} \quad (5)$$

for the contained and semicontained events in good agreement with our earlier publication [23], and

$$R = 0.99 \pm 0.13 \text{ (stat.)} \pm 0.08 \text{ (syst.)} \quad (6)$$

for the total neutrino induced event sample is consistent with unity. The discussion on the systematic errors is already given in Ref. [23].

5.1 Neutrino interactions inside the detector

In section 3.1 we have demonstrated that the selected contained and semicontained event sample is completely due to neutrino interactions inside the detector. No indication for any relevant contaminations by other sources has been found. Together with our previous publications [11, 23] it may be concluded that the Monte Carlo simulated events give a satisfactory description of our data. Therefore the Monte Carlo is used to perform a regularized unfolding of the data. This procedure allows to correct the data for efficiencies, misidentification and detector resolution effects in an unbiased way. Based on the two different data samples separated according to the lepton type identification as detailed in Ref. [11] the distribution of the visible energy is unfolded to obtain the absolute ν_μ and ν_e spectra of atmospheric neutrinos averaged over the zenith angle. The spectra are shown in Fig. 6 and 7 as a function of the neutrino energy E_ν for the atmospheric ν_μ and ν_e flux, respectively. The results on the ν_e and ν_μ fluxes obtained by the unfolding of the contained and semicontained charged current events are listed in Tabs. 6 and 7 of appendix A.

In Fig. 8 the ν-fluxes are compared to various theoretical calculations [15-20]. The neutrino flux predicted by [19] is systematically below the atmospheric neutrino flux both for ν_μ and ν_e while the prediction of [17] for the ν_e flux is systematically to high. A function of the form

$$\Phi(E_\nu) = \eta\, \Phi_{theo}(E_\nu) \quad (7)$$

is fitted to the ν_μ and ν_e spectra. Here Φ_{theo} denotes the theoretical neutrino flux predictions within the different calculations and η is a free parameter for the absolute overall normalization. The results of these fits are summarized in the Tab. 2 for the ν_μ and the ν_e flux and the combination of both fluxes, respectively[4]. Within the accuracy of our measurement good agreement is observed for the predictions of Ref. [15-18,20] for the ν_μ flux in absolute normalization as well as in the energy dependence of the ν_μ spectrum. The fits of the different calculations to the atmospheric ν_e

[4] It should be stressed that the experimental errors of the unfolded data are dominated by the energy resolution of the detector. In contrast to Eq. (5) this fit is more sensitive on the slope of the spectra than on the absolute rate.

Table 2. Results of the fits of the form $\Phi(E_\nu) = \eta\, \Phi_{theo}(E_\nu)$ for different models to the absolute ν_μ, ν_e and $\nu_\mu + \nu_e$ flux as derived from the contained and semicontained events observed in the Fréjus detector.

		ν_μ		ν_e		$\nu_\mu + \nu_e$	
Model	Ref.	η	χ^2/NDF	η	χ^2/NDF	η	χ^2/NDF
Gaisser et al.	16						
& Volkova	15	1.05 ± 0.13	6.6/6	0.77 ± 0.13	6.7/6	0.90 ± 0.12	16.6/13
Mitsui et al.	18	0.93 ± 0.13	6.5/6	0.77 ± 0.13	4.5/6	0.85 ± 0.08	15.6/13
Butkevich et al.	17	0.80 ± 0.22	3.6/3	0.48 ± 0.12	0.5/3	0.61 ± 0.10	7.5/7
Treichel	19	1.7 ± 0.4	12.1/3	2.6 ± 0.6	2.2/3	1.8 ± 0.3	16.4/7
Lipari	20	0.95 ± 0.17	3.4/3	0.57 ± 0.13	0.5/3	0.73 ± 0.13	7.6/7

Table 3. Compilation of the relative systematic uncertainties in the determination of the absolute ν_μ and ν_e spectra as a function of E_ν.

	ν_μ spectrum			ν_e spectrum		
	300 MeV	1 GeV	>10 GeV	300 MeV	1 GeV	>10 GeV
$\sigma(\nu N)$	0.30	0.20	0.15	0.30	0.20	0.15
$\Phi(\nu)/\Phi(\overline{\nu})$	0.02	0.02	< 0.01	0.05	0.03	< 0.02
geographical topology	< 0.01	< 0.01	< 0.01	0.02	0.03	0.05
trigger + nuclear effects	0.08	0.05	< 0.03	0.12	0.06	< 0.03
effective target volume	0.06	0.03	0.05	0.06	0.03	0.05
detector simulation	0.05	0.05	0.05	0.05	0.05	0.05
lepton type identification	0.05	0.02	0.05	0.05	0.02	0.05
neutral current contribution	0.02	0.01	< 0.01	0.04	0.02	< 0.01
total	0.32	0.22	0.17	0.34	0.22	0.18

spectrum yield reasonable values for the χ^2/NDF but the absolute flux predictions are systematically above the observation except for the calculation of Ref. [19]. The deviation from $\eta = 1$ for the other predictions with respect to the ν_e spectrum is due to its behaviour for $E_\nu > 1$ GeV where the atmospheric ν_e flux is roughly a factor of 2 below the different model calculations at a statistical significance of more than 2 standard deviations.

The systematic errors in the determination of the absolute neutrino spectra based on the contained and semicontained events are summarized in Tab. 3. The major uncertainties arise from our lake of knowledge of the neutrino cross section, of the nuclear effects in the iron nucleus and the exact understanding of the threshold behaviour of the trigger for ν_e interactions below 800 MeV. All these uncertainties affect mainly the neutrino spectra at low energies. In addition minor contributions are obtained due to the determination of the effective target volume and the simulation of the neutrino interactions in the detector.

In the energy range accessible by the contained and semicontained events the ν_e flux is completely due to muons decaying in the atmosphere. Especially at high energies the ν_e flux is thus influenced by the height of the mountains around the experiment preventing penetrating muons from decaying in flight. To study the effect of the geographical topology on the absolute neutrino flux at Fréjus the CORSIKA air shower simulation program [41] together with the decay spectra including muon polarization as given in Ref. [20] is used to calculate neutrino spectra produced by primary cosmic rays at different zenith angles at sea level and at an altitude of 3000 meters corresponding approximately to the height of the mountains at Fréjus. While the ν_μ flux is not affected by the geographical topology a reduction of 5%

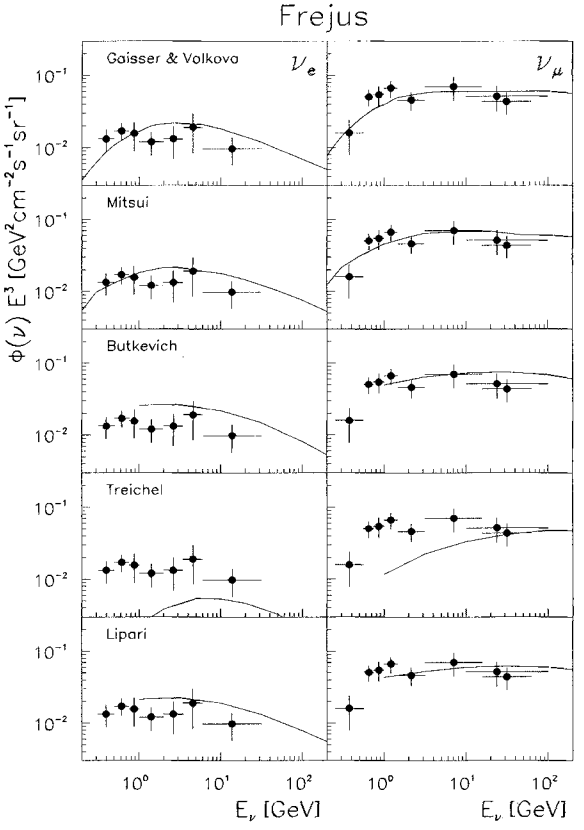

Fig. 8. Comparison of the absolute ν_e (left) and ν_μ spectrum (right) multiplied by $E^{3.0}$ as obtained from the contained and semicontained ν-interactions in the Fréjus detector averaged over the zenith angle with different neutrino flux calculations.

on the ν_e flux averaged over the zenith angle is observed for $E_\nu \approx 10$ GeV.

The different contributions to the systematic error are added in quadrature leading to the energy dependent total systematic error given in Tab. 3. Compared to the experimental errors due to statistics and resolution effects as obtained by the unfolding procedure the energy dependent part of the total systematic error is small enough to be neglected in the comparison of the atmospheric neutrino spectra to the different theoretical calculations. The overall absolute neutrino flux normalization error is estimated to be of the order of 20 %, mainly due to the uncertainties of the total νN cross section, in agreement with our previous studies performed in Ref. [11, 23, 35]. For the estimation of the systematic errors on the ν_e spectrum it is assumed that the ν_e cross section is identical to the ν_μ cross section independent of the neutrino energy. Since the influence of the induced formfactors on the quasi elastic scattering cross section is still unknown, this assumption may be an oversimplification for low neutrino energies where the contribution of this process dominates the νN cross section.

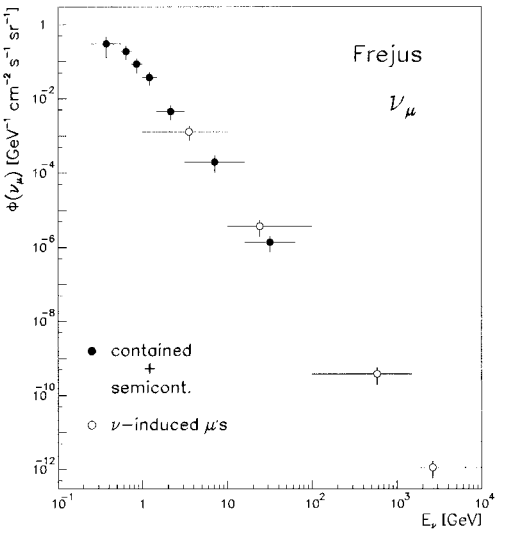

Fig. 9. The absolute ν_μ-spectrum obtained from the total neutrino induced event sample averaged over the zenith angle.

5.2 Neutrino induced muons

For neutrino energies $E_\nu \gg 1$ GeV the differential spectra of the atmospheric neutrino flux has been parametrized by [15][5]

$$\Phi_\nu = \Phi_0 \, E^{-\alpha} \left[\frac{1}{1 + 6\,E_\nu / E_\pi(\Theta)} + \frac{0.213}{1 + 1.44\,E_\nu / E_{K^\pm}(\Theta)} \right], \qquad (8)$$

where $E_\pi(\Theta)$ and $E_{K^\pm}(\Theta)$ are the zenith angle dependent critical energies[6] accounting for the $\pi^\pm$ and $K^\pm$ decay length, respectively. Within the experimental errors this simple parametrization leads to a good description of our data for $E_\nu \geq 3$ GeV.

From the observed number of the contained and semicontained charged current ν_μ interactions and the through-going horizontal muon events given in Tab. 1 a value of $r_{hori}^{cont} = 2.84 \pm 0.50$ is obtained which has to be compared with the Monte Carlo expectation of $r_{hori}^{cont} = 3.10$ for a spectral index of $\alpha = 2.69$ using the flux parametrization according to Eq. (8). The experimental value on r_{hori}^{cont} yields a spectral index $\alpha = 2.67 \pm 0.05$.

Using the observed numbers of candidate events of upward-going stopping muons and of through-going horizontal muon events a value of $r_{hori}^{stop} = 1.09 \pm 0.23$ is observed. As already discussed in the text the upward-going stopping muons candidates receive significant contribution from misidentified through-going atmospheric muons (11 events) and from semicontained ν_μ interactions with only one visible track (11.7 events expected). The rate of the latter background also depends on the spectral index α of the ν_μ flux. As shown in Figs. 4 and 5 the neutrino energy range of interest for the upward-going stopping muons is independently covered by the contained and semicontained events which allows to determine the contamination due to semicontained ν_μ interactions.The comparison with the Monte Carlo expectations for $r_{hori}^{stop}(\alpha)$ for different values of α leads to $\alpha = 2.65 \pm 0.06$.

The analysis of the energy loss of horizontal muons due to pair production, bremsstrahlung and photoproduction is based on reconstructed showers with $E_{sh} \geq 300$ MeV only. It turns out that in this case the systematic uncertainties in the determination of the spectral index α are minimized by simply counting the number of reconstructed showers per track length. We obtain $dN_{sh}^{300}/dx = (6.4 \pm 1.3_{stat} \pm 0.3_{syst})\ 10^{-2}$ m^{-1}, where the systematic error accounts for the uncertainty in the absolute energy calibration of electromagnetic showers [32]. Comparing this value to Monte Carlo predictions for different spectral indices one gets $\alpha = 2.62 \pm 0.15$. The combination of both independent measurements leads to a spectral index for the atmospheric ν_μ-flux of

$$\alpha = 2.66 \pm 0.05 \text{ (stat.)} \pm 0.03 \text{ (syst.)}. \qquad (9)$$

Based on this value an absolute normalization factor of

$$\Phi_0 = (2.5 \pm 0.2 \text{ (stat.)} \pm 0.3 \text{ (syst.)})\ 10^{-2} \text{ cm}^{-2}\,\text{s}^{-1}\,\text{sr}^{-1}\,\text{GeV}^{\alpha-1} \qquad (10)$$

for the ν_μ spectrum in Eq. (8) is obtained from the total rate of ν_μ induced charged current events. The discussion on the systematic error is given below (Tab. 5). Both, the spectral index α and the absolute neutrino flux normalization Φ_0 are in good agreement with the prediction of Ref. [15] where $\alpha = 2.69$ and $\Phi_0 = 2.85 \times 10^{-2}$ cm^{-2}s^{-1}sr^{-1}GeV$^{\alpha-1}$ is quoted.

In the next step the neutrino induced muon data is unfolded using the total visible energy loss of the muons in the detector in order to obtain the absolute ν_μ spectrum for 1 GeV $< E_\nu <$ 10 TeV. The result is shown in Fig. 9

[5] The parametrization of Volkova is chosen because it allows for a simple description of the data which is not possible for the other theoretical calculations. The unfolded spectra shown in Fig. 6 and 7 are not affected by this parametrization.

[6] $E_\pi(\Theta)$ and $E_{K^\pm}(\Theta)$ are detailed in ref[15].

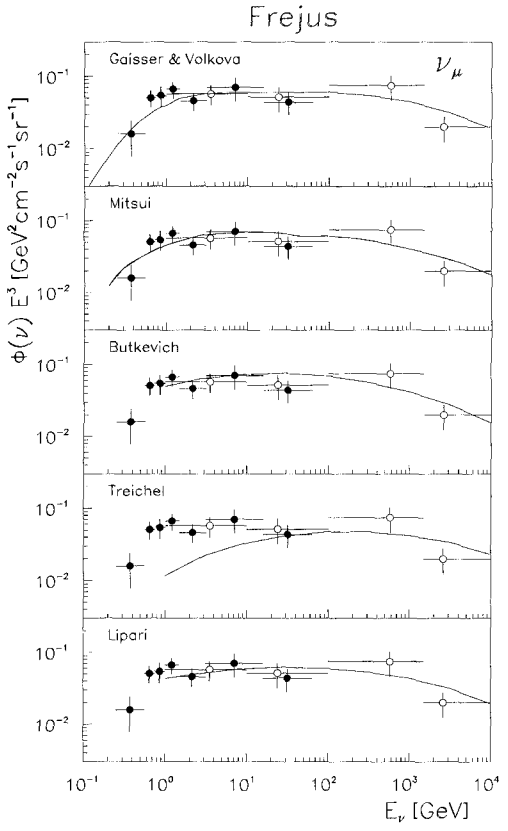

Fig. 10. The absolute ν_μ spectrum multiplied by $E^{3.0}$ as obtained from the contained, semicontained ν-interactions in the Fréjus detector and the neutrino induced muons averaged over the zenith angle compared to different neutrino flux calculations.

Table 4. Results of the fits of the form $\Phi(E_\nu) = \eta\,\Phi_{theo}(E_\nu)$ for different models to the absolute ν_μ flux derived from the ν_μ interaction inside the detector and the ν_μ induced muons.

		ν_μ	
Model	Ref.	η	χ^2/NDF
Gaisser et al.	16		
& Volkova	15	0.95 ± 0.11	11.5/10
Mitsui et al.	18	0.89 ± 0.10	9.7/10
Butkevich et al.	17	0.80 ± 0.11	6.5/7
Treichel	19	1.06 ± 0.15	27.5/7
Lipari	20	0.88 ± 0.12	8.2/7

Table 5. Compilation of the relative systematic uncertainties in the determination of the absolute ν_μ spectrum as a function of E_ν for 5 GeV $\leq E_\nu \leq$ 5 TeV.

	ν_μ spectrum			
	5 GeV	50 GeV	500 GeV	5 TeV
$\sigma(\nu N)$	0.18	0.03	0.05	0.10
$\Phi(\nu)/\Phi(\overline{\nu})$	0.01	0.01	0.02	0.02
$\sigma(pp \rightarrow c\overline{c})$	-	-	0.02	0.10
energy loss	0.06	0.06	0.088	0.094
μ_{hori} pointing	0.19	0.09	0.07	0.07
μ_{stop} pointing	0.04	-	-	-
ν_μ-acceptance μ_{hori}	0.09	0.07	0.10	0.10
ν_μ-acceptance μ_{stop}	0.04	-	-	-
total μ_{hori}	0.28	0.13	0.16	0.21
total μ_{stop}	0.20	-	-	-

together with the ν_μ spectrum obtained from the analysis of the contained and semicontained events described in the previous section. The absolute ν_μ spectrum derived form the neutrino induced muons fits well the spectrum as determined by the contained and semicontained events in the region 1 GeV $< E_\nu <$ 60 GeV where both data sample overlap. The results on the absolute ν_μ flux as obtained by the unfolding of the neutrino induced muon events are included in Tab. 7 of appendix A. The comparison of the absolute ν_μ-flux with different theoretical calculation [20-25] for 300 MeV $< E_\nu <$ 10 TeV is shown in Fig. 10. The results of fits to the ν_μ-spectrum according to Eq. (7), based on the experimental errors, are summarized in Tab. 4. Within the accuracy of our experiment the theoretical predictions are in reasonable agreement with the absolute flux measurement both in normalization and in the slope of the spectrum except of Ref. [19] as already observed in the analysis based on the contained and semicontained events only.

In Tab. 5 a compilation of the systematic uncertainties in the ν_μ-flux determination using the ν_μ-induced events is given. In general three different categories of uncertainties have to be considered, namely:

a) the error on the effective νN cross section, denoted by $\sigma(\nu N)$ and $\Phi(\nu)/\Phi(\overline{\nu})$. The error on the neutrino cross section also accounts for the uncertainties due to our lack of knowledge on the parton densities in the nucleon as briefly discussed in section 4.

b) the uncertainties on the effective target volume determined by the energy loss parameters given in Eq. (3) and

c) the influence of the restriction in the usable solid angle for the identification of neutrino induced muons. Here the effect of the pointing accuracy of the muons, including the kinematics at the neutrino vertex, and the effect of the differences in the zenith angle dependence within different models (ν_μ-acceptance) has to be considered.

For $E_\nu <$ 10 GeV where the flux measurement is dominated by the upward-going stopping muons the systematic error is mainly due to the experimental uncertainties on the total neutrino cross section while at higher energies the different sources contribute equally to the total systematic error.

At higher energies, i.e. $E_\nu >$ 1 TeV, the ν_μ-flux may receive a sizeable contribution due to charm production. In contrast to the K's, and π's the charmed particles decay almost completely before interacting even at high energies because of their short lifetime leading to an isotropic contribution to the ν_μ and μ flux. For $E_\mu \geq 5$ TeV the prompt μ-flux from charm decay is found to be $\approx 10\%$ of the vertical μ-flux as derived from the analysis of the depth intensity relation for atmospheric muons [29]. This value can be converted into an uncertainty on the ν_μ-flux measurement, averaged in zenith angle, of 10% for E_{ν_μ} = 5 TeV.

The total systematic error on the ν_μ-flux determination based on the neutrino induced muons as given in Tab. 5 shows only a small energy dependence if one takes into account that for $E_\nu <$ 10 GeV the ν_μ-spectrum is mainly determined by the upward-going stopping muons. The en-

ergy independent part of the total systematic uncertainties levels to 13%.

6 Discussion and conclusions

In this article a combined analysis of the final event samples of neutrino interactions inside the detector, of upward-going stopping muons and of horizontal muons recorded in the Fréjus experiment is presented. It is the combination of these different measurements which enabled us to determine the absolute atmospheric neutrino spectra in the energy range 320 MeV$< E_{\nu_e} <$ 30 GeV for electron neutrinos and 250 MeV$< E_{\nu_\mu} <$ 10 TeV for muon neutrinos for the first time. The determination of the ν_μ spectrum up to 10 TeV is of specific interest for experiments working in the field of high energy neutrino astronomy. Consequences on models predicting an isotropic extraterrestrial neutrino flux will be discussed in a separate paper [33]. Using the parametrization of Volkova we obtain a spectral index of $\alpha = 2.66 \pm 0.05$ and a flux normalization factor of $\Phi_0 = (2.5 \pm 0.2_{stat} \pm 0.3_{syst}) \times 10^{-2}\text{cm}^{-2}\text{s}^{-1}\text{sr}^{-1}\ \text{GeV}^{\alpha-1}$ which are both in good agreement with the values given in [15].

Various theoretical calculations have been compared to the absolute flux measurements presented in this paper. Although the statistical errors are still quite large the data gives significant constraints on neutrino flux calculations especially because of the large range in neutrino energy covered by the experiment. Even by including the systematic uncertainties of the absolute measurement the ν_e flux is found to be systematically below the different predictions at more than two standard deviations for $E_\nu > 1$ GeV (Fig. 8 and Tab. 2). Although in general an overall normalization uncertainty of about 20% is quoted for the flux calculations, the relative normalization between the ν_μ and the ν_e flux is assumed to be accurate to the 5% level. The calculations of Ref. [15, 16, 18] on the relative normalization of the fluxes agree reasonably well with our measurement of the absolute spectra while the predictions of Ref. [17, 20] are found to be only in marginal agreement (about two standard deviations) if the understanding of the relative normalization between the ν_μ and the ν_e flux is as good as commonly thought. The measurements of the ν_μ and the ν_e-flux are both in contradiction to the calculation of Ref. [19]. We conclude from our comparison that for ν_μ energies larger than 100 Gev the approximation of [19] becomes valid. This approximation may be worse in case of the ν_e flux.

Since the rate of neutrino events observed in the Fréjus experiment is in good agreement with the Monte Carlo expectation for both charged current ν_e and ν_μ interactions there is no evidence for neutrino oscillations from this analysis consistent with our earlier publication [23]. However there is still some room left for an interpretation of the abnormal n_μ/n_e ratio as reported by Ref. [12, 13, 22, 24] in the framework of ν_μ-ν_τ-oscillations that is consistent with our data.

Recently Kamiokande reported on an abnormal ratio n_μ/n_e for contained and semicontained neutrino events with a visible energy $E_{vis} > 1.3$ GeV [22]. The basic feature of this data is an excess of electron type events of $(n_e)_{data}/(n_e)_{MC} = 1.43 \pm .15$. In terms of ν_μ-ν_τ-oscillations this result may only be considered if one assumes the n_e-excess to be due to a genuine higher atmospheric ν_e flux as predicted from calculations for $E_\nu > 1$ GeV. Such an increase in the ν_e flux contradicts the flux measurement presented in the present paper at more than 99% confidence level, even by restricting our data to $E_\nu \geq 1.5$ GeV. Geomagnetic effects which produce significant differences in the neutrino spectra at Kamioka and Fréjus at low energies are too small for $E_\nu \geq 1.5$ GeV to be responsible for such a big difference in the ν_e flux at both sites necessary to get agreement between our ν_e flux measurement and the ν_μ-ν_τ hypothesis for the Kamiokande data.

Comparing our analyses with the analyses performed by the experiments claiming evidence for an abnormal ratio of muon type over electron type neutrino interactions in their apparatus [12, 13, 22, 24] two major differences have to be realized

a) the analyses of Fréjus are based on the complete neutrino sample accessible by the experiment while the other groups have, mainly due to technical reasons, restricted their analyses to the quasi-elastic neutrino scattering events only,
b) the Fréjus detector has been located at a depth of more than 4700 hg/cm^2, while the experiments which have reported evidence for an abnormal n_μ/n_e ratio are operating at shallower depths of less than 2500 hg/cm^2.

The experimental knowledge [43] as well as the theoretical understanding [44] of the quasi-elastic neutrino scattering cross section is still very limited. For the analysis presented in this paper the quasielastic scattering channels contribute only ≈30% to the contained and semicontained events while the upward-going stopping muons and the horizontal through-going muons are nearly completely due to deep inelastic neutrino scattering. Since the physics of deep inelastic scattering is much better understood and the total neutrino scattering cross section is much better known than the quasielastic scattering process alone our analyses should be almost free from the uncertainties on the quasielastic scattering cross section. This may also explains why the searches for neutrino oscillations based on the analyses of upward-going, horizontal through-going or stopping muons performed by several experiments [25, 26, 27] failed to find evidence for neutrino oscillations as suggested by the apparent n_μ/n_e anomaly as primarily reported by Kamiokande although theses analyses have large systematic errors since they have to rely completely on absolute neutrino flux calculations.

Due to the shallow depths of IMB, Kamiokande and Soudan-II the atmospheric muon flux in these experiments is more than a factor of 20 higher as compared to the flux at the Fréjus laboratory. Consequently in the former experiments a significant high energetic neutron flux originating from interactions of muons in the surrounding rock near the detector could be expected. The production of π^0's by interactions of these neutrons in the detector may lead to an excess of electron like events thus explaining the apparent n_μ/n_e anomaly [45]. For the Fréjus experiment we have

demonstrated that this background source is expected to be negligible.

The accuracy in the determination of the absolute neutrino spectra obtained in the present analysis is mainly limited by the small statistics available in the Fréjus experiment. Significant improvements on the experimental knowledge of the neutrino fluxes would require much larger statistics taken with a detector having features at least similar to those of the Fréjus detector. None of the underground experiments under construction or being built in the near future will meet these requirements. Moreover the systematic uncertainties will become important as soon as much larger statistics would be available. A better understanding of the neutrino nucleon cross section would then be needed.

Acknowledgement. It is a pleasure to thank the French and Italian authorities of the Fréjus tunnel, SFTRF and CITAF, for their co-operation. We are grateful to the technicians for their invaluable support in the detector maintenance. K.D. would like to thank D. Haidt for fruitful discussions and valuable comments, the DESY directorate for the hospitality and the Ministerium für Wissenschaft und Forschung Nordrhein-Westfahlen for its support.

A Absolute ν_e and ν_μ fluxes of atmospheric neutrinos

Tables 6 and 7 summarize the measured values and errors of the absolute ν_e and ν_μ fluxes for the different neutrino energies as determined by the analysis presented in this paper. The fluxes are averaged in zenith angle.

Table 6. Absolute ν_e flux as obtained by the unfolding of the contained and semicontained charged current ν_e event averaged in zenith angle.

		ν_e spectrum	
$E_\nu^{min} - E_\nu^{max}$ [GeV]	$\langle E_\nu \rangle$	Φ_ν [GeV^{-1}cm^{-2}s^{-1}sr^{-1}]	$\Delta\Phi_\nu$
0.32 – 0.50	0.40	$2.1\ 10^{-1}$	$7.2\ 10^{-2}$
0.50 – 0.76	0.62	$7.3\ 10^{-2}$	$1.9\ 10^{-2}$
0.76 – 1.00	0.87	$2.4\ 10^{-2}$	$1.0\ 10^{-2}$
1.00 – 2.00	1.41	$4.3\ 10^{-3}$	$1.6\ 10^{-3}$
2.00 – 3.50	2.63	$7.3\ 10^{-4}$	$3.5\ 10^{-4}$
3.50 – 6.00	4.57	$2.0\ 10^{-4}$	$1.1\ 10^{-4}$
6.00 – 31.6	13.8	$3.7\ 10^{-6}$	$1.5\ 10^{-6}$

Table 7. Absolute ν_μ flux as obtained by the unfolding of the contained and semicontained charged current ν_μ events and the neutrino induced muons averaged in zenith angle.

		ν_μ spectrum	
$E_\nu^{min} - E_\nu^{max}$ [GeV]	$\langle E_\nu \rangle$	Φ_ν [GeV^{-1}cm^{-2}s^{-1}sr^{-1}]	$\Delta\Phi_\nu$
0.25 – 0.56	0.38	$3.0\ 10^{-1}$	$1.5\ 10^{-1}$
0.56 – 0.74	0.65	$1.9\ 10^{-1}$	$5.0\ 10^{-2}$
0.74 – 1.00	0.86	$8.6\ 10^{-2}$	$2.7\ 10^{-2}$
1.00 – 1.48	1.22	$3.7\ 10^{-2}$	$9.7\ 10^{-3}$
1.48 – 3.16	2.16	$4.5\ 10^{-3}$	$1.3\ 10^{-3}$
1.00 – 10.0	3.54	$1.3\ 10^{-3}$	$4.0\ 10^{-4}$
3.16 – 15.9	7.1	$2.0\ 10^{-4}$	$7.2\ 10^{-5}$
10.0 – 100	24.0	$3.7\ 10^{-6}$	$1.4\ 10^{-6}$
15.9 – 63.1	31.6	$1.4\ 10^{-6}$	$4.7\ 10^{-7}$
100 – 1500	580	$3.8\ 10^{-10}$	$1.5\ 10^{-10}$
1500 – 10000	2610	$1.1\ 10^{-12}$	$4.4\ 10^{-13}$

References

1. M.L. Cherry et al.: Phys. Rev. Lett. 47 (1986) 167
2. M.R. Krishnaswamy et al.: Nuovo Cim. 9C (1986) 167
3. S. Seidel et al., IMB Coll.: Phys. Rev. Lett 61 (1988) 2522
4. K.S. Hirata et al., Kamiokande Coll.: Phys. Lett. B 220 (1989) 308; Phys. Lett B280 (1992) 146
5. G. Battistoni et al., NUSEX Coll.: Phys. Lett 133 B (1983) 454
6. C. Berger et al., Frejus Coll.: Nucl. Phys. B 313 (1989) 509; Z. Phys. C 50 (1991) 385; Phys. Lett. B 269 (1991) 227
7. T.J. Phillips et al., HPW Coll.: Phys. Lett. B 224 (1989) 348
8. R.M. Bioanta et al., IMB Coll.: Phys. Rev. D 38 (1988) 768
9. K.S. Hirata et al., Kamiokande Coll.: Phys Lett B 205 (1988) 416
10. M. Aglietta et al., NUSSEX Coll.: Europhys. Lett. 8 (1989) 611
11. C. Berger et al., Fréjus Coll.: Phys. Lett. B 227 (1989) 489
12. K.S. Hirata et al., Kamiokande Coll.: Phys. Lett. B 280 (1992) 146;K. Nishikawa: Proceedings of the XVI International Conference on Neutrino Physics and Astrophysics, Eilat, 1994.
13. D. Casper et al., IMB Coll.: Phys. Rev. Lett. 66 (1991) 2561; R.C. Svoboda: Proceedings of the XVI International Conference on Neutrino Physics and Astrophysics, Eilat, 1994
14. S.W. Barwick et al., AMANDA Coll.: Contribution to the 5^{th} International Workshop on Neutrino Telescopes, Venice, 1993; I.A. Belolaptikov et al., BAIKAL Coll.: Contribution to the 5^{th} International Workshop on Neutrino Telescopes, Venice, 1993; DUMAND proposal, HDC 2-88, 1988; E. Anassontzis et al., NESTOR Coll.:Contribution to the 5^{th} International Workshop on Neutrino Telescopes, Venice, 1993
15. L.V. Volkova: Sov. J. Nucl. Phys. 31 (1980) 784
16. T.K. Gaisser, T. Stanev and G. Barr: Phys. Rev. D 38 (1988) 85; G. Barr, T.K. Gaisser and T. Stanev: Phys. Rev. D 39 (1989) 3532
17. A.V. Butkevich, L.G. Dedenko and I.M. Zheleznykh: Sov. J. Nucl. Phys. 50 (1989) 90
18. K. Mitsui, Y. Minorikawa and H. Komori: Nuovo Cim. 9C (1986) 995
19. M. Treichel: Z. Phys. C 54 (1992) 469
20. P. Lipari: Astrop. Phys. 1 (1993) 195
21. E.V. Bugaev and V.A. Naumov: Phys.Lett. B 232 (1989) 391; M. Honda et al.: Phys. Lett. B 248 (1990) 193; H. Lee and Y.S. Koh: Nuov. Cim. 105 B (1990) 883; M Kawasaki and S. Mizuta: Phys Rev. D 43 (1991) 2900; D. Perkins: Astrop. Phys. 2 (1994) 249
22. Y. Fukuda et al., Kamiokande Coll.: Phys. Lett. B 335 (1994) 237
23. C. Berger et al., Fréjus Coll.: Phys. Lett. B 245 (1990) 305
24. M.C. Goodmann: Proceedings of the XVI International Conference on Neutrino Physics and Astrophysics, Eilat, 1994
25. R. Becker-Szendy et al., IMB Coll.: Phys. Rev. Lett. 69(1992) 1010
26. M.M. Boliev et al.: Contribution to the 3^{rd} International Workshop on Neutrino Telescopes, Venice, 1991, p235
27. Y. Oyama et al., Kamiokande Coll.: Phys. Rev. D 39 (1989) 481
28. V. Blobel: DESY-Preprint, DESY 84-118
29. W. Rhode: thesis 1993, WUB-DIS 93-11, University of Wuppertal
30. F. Ellenberger: Etude Géologique du pays de la Vanoise, edited by Bureau de Recherches Géologiques et Miniéres, Paris 1958 (Mém. Carte Géol. Fr., Paris, 1958); M.P. Gwinner: Geologie der Alpen, Stuttgart, 1978
31. C. Berger et al., Fréjus Coll.: Phys Rev D40 (1989) 2163
32. C. Berger et al., Fréjus Coll.: Nucl. Instrum. Methods A262 (1987) 463
33. W. Rhode et al.: to be published
34. Yi Wei: thesis 1993, WUB-DIS 93-8, University of Wuppertal
35. C. Berger et al., Fréjus Coll.: Z. Phys. C 50 (1991) 509
36. C. Berger et al., Fréjus Coll.: Nucl. Instrum. Methods A302 (1991) 406
37. H. Faissner et al.: Phys. Rev. Lett. 41 (1978) 213
38. E. Eichten et al.: Rev. Mod. Phys. 56 (1984) 579; D.W. McKay and J.P. Ralston: Phys. Lett. B 167 (1986) 103;
39. J. Kwiecinski et al.: Phys. Rev. D 42 (1990) 3645; J.G. Morfin and W.K. Tung: Z. Phys. C 52 (1991) 13; J.F. Owens: Phys. Lett. B 266 (1991) 126; M. Glück, E. Reya and A. Vogt: Z. Phys. 53 (1992) 127
40. I. Abt et al., H1 Collab.: Nucl. Phys. B 407 (1993)515; M. Derrick et al., ZEUS Collab.: Phys. Lett. B 316 (1993) 412
41. J.N. Capdevielle et al.: KfK-Preprint, KfK-4998, KfK Karlsruhe, 1992

42. R. Becker-Szendy et al., IBM Coll.: Phys. Rev. Lett. 69 (1992) 1010
43. A. Orkin-Lecourtois and C.A. Piketty: Nuov. Cim. 50A (1967) 927; M. Holder et al.: Nuov. Cim. 57A (1968) 339; T. Eichten et al.: Phys. Lett. B46 (1973) 274; W.A. Mann et al.: Phys. Rev. Lett. 31 (1973) 844; I. Budagov et al.: Lett. Nouv. Cim. 2 (1969) 689; S. Bonetti et al.: Nuov. Cim. 38A (1977) 260; M. Pohl et al.: Lett. Nuov. Cim. 26 (1979) 332; G. Fanourakis et al.: Phys. Rev. D21 (1980) 562; N. J. Baker et al.: Phys. Rev. D23 (1981) 2499; S.V. Belikov et al.: Sov. J. Nucl. Phys. 41 (1985) 589; S. J. Barish et al.: Phys. Rev. D16 (1977) 3103
44. C.H. Llewelyn Smith: Phys. Rep. 3C (1971) 261
45. O.G. Ryazhskaya: Gran Sasso-Preprint, LNGS - 94/110

This article was processed by the author using the LaTeX style file *pljour2* from Springer-Verlag.